# Response to two Reviewers and Editor

Reviewer 1

The authors have made substantial changes to the manuscript. I would suggest the authors make minor revisions to make the manuscript easier to read.

Response: We thank the reviewer for the valuable time and great efforts in evaluating our work. Detailed responses to the constructive comments are as follows.

1. Figure 2. "monthly wind verctor?". Monthly-climatological or May 2012?

Response: Yes. Monthly mean of May 2012. We noted this information in Figure 2.

2. Figure 4. What periods of data are used for SODA, HYCOM, and WOA?

Response: We used monthly mean data of May 2012. We added this information in Figure 4.

3. Could you highlight the 22 kg/m$^3$ isopycnal in Figure 4?

Response: We labeled the 22 kg/m$^3$ isopycnal in new Figure 4.

4. "comparison implies that the year 2002 is an anomaly year for the distributions of ASHSW, PGW and RSW." Could you give some interpretation here? Maybe you could add a sub-graph to show the wind anomaly in May 2012 in Fig. 2, if the conclusion "the ventilation is induced by surface wind" is correct.

Response: We therefore look into the inter-annual variation of wind anomaly. For the 7-year averaged monthly mean wind vorticity (Figure A1), a negative vorticity from wind is observed in Arabian Basin. Then in the year 2002 (Figure A2), the negative vorticity is further enhanced (negative anomaly) in Arabian Basin. In contrast, in some other years, it is relatively weak (positive anomaly). The negative wind vorticity input is the main reason of south movement of ASHSW (Schott et al., 2009; Sverdrup Balance). However, the description is not quantitative, we hope to do more work in the future.

Schott, F. A., Xie, S. P., and McCreary Jr. J. P.: Indian Ocean circulation and climate variability, Reviews of Geophyscis, 47, RG1002, 2009.

5. Too many abbreviations are not benefit for reading.

Response: We deleted the abbreviations including IO (Indian Ocean), IOD (Indian Ocean Dipole), RAMA (Research Moored Array for African-Asian-Australian Monsoon Analysis and Prediction), ADT ( absolute dynamic height), IEW (Indian Equatorial Water) and ASW (Arabian Sea Water).

6. Figure 6. As you discussed Fig. 6e first, and then Fig. 6c and Fig. 6a, you may want to rearrange the subgraphs.

Response: [Page 12-13, Change-Track-Mode revised manuscript] The sequence in Figure 6 is consistent with the geographic distribution. Therefore, we rearranged the text instead.

7. Please add some information about the "starting/ending point" in Figure 6 caption.

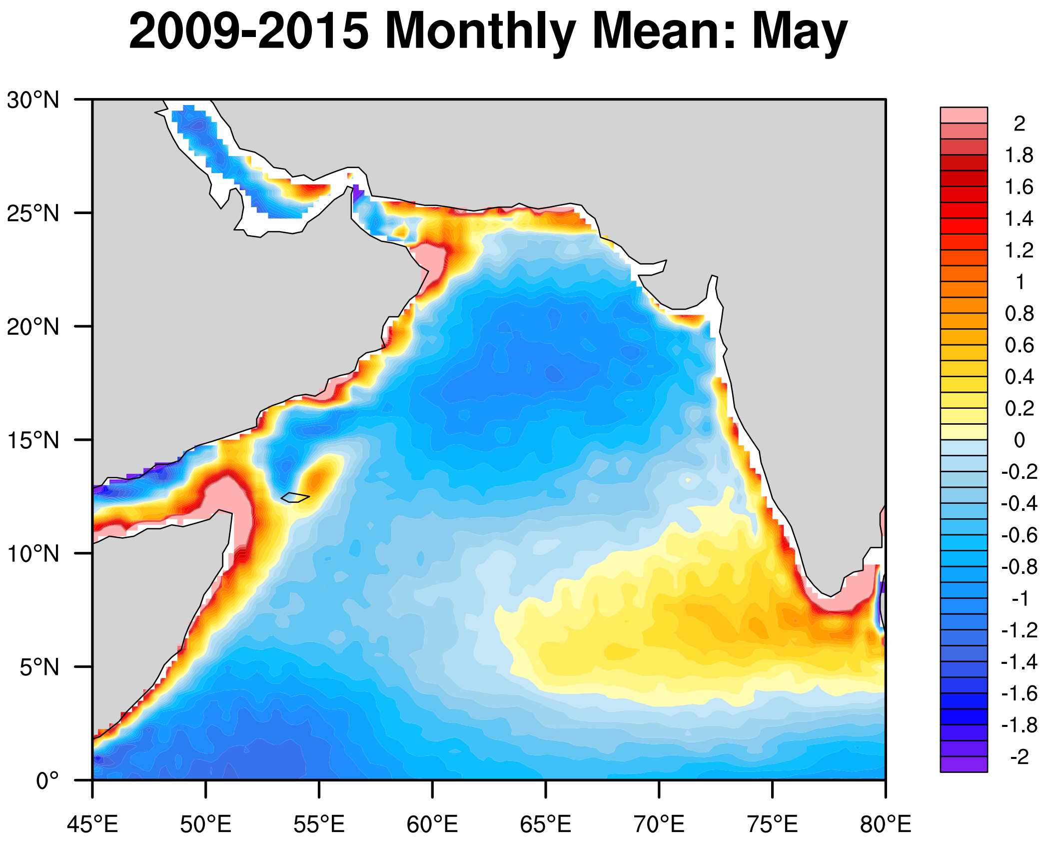


Figure A1: 7-year averaged monthly mean wind vorticity (2009-2015; May).

Response: Corrected.

8. "We set some passive tracers along the CR." Do you mean you set the traces along the CTD/XCTD stations shown in Fig. 1? If so, it would be helpful to show the section in Figure 6.

Response: We added the section in Figure 6.

9. To me, the title is not appropriate.

Response: Yes, the title looks general. But the time and space define the specificity of the study. We kept the title finally.

10. The revised "Introduction" is much better than the former. I noticed you raised several questions: pathways of water masses, and mechanics for their moves are not clear. The meso-scale eddies and planetary waves are not sufficiently observed. The internal dynamics of planetary wave is not sufficiently addressed. I also noticed you added several sentences to state the purpose/content of this manuscript: "First, hydrographic survey takes a snapshot on the water mass, and gives an evidence on the activity of water mass. Second,?". I feel like there is

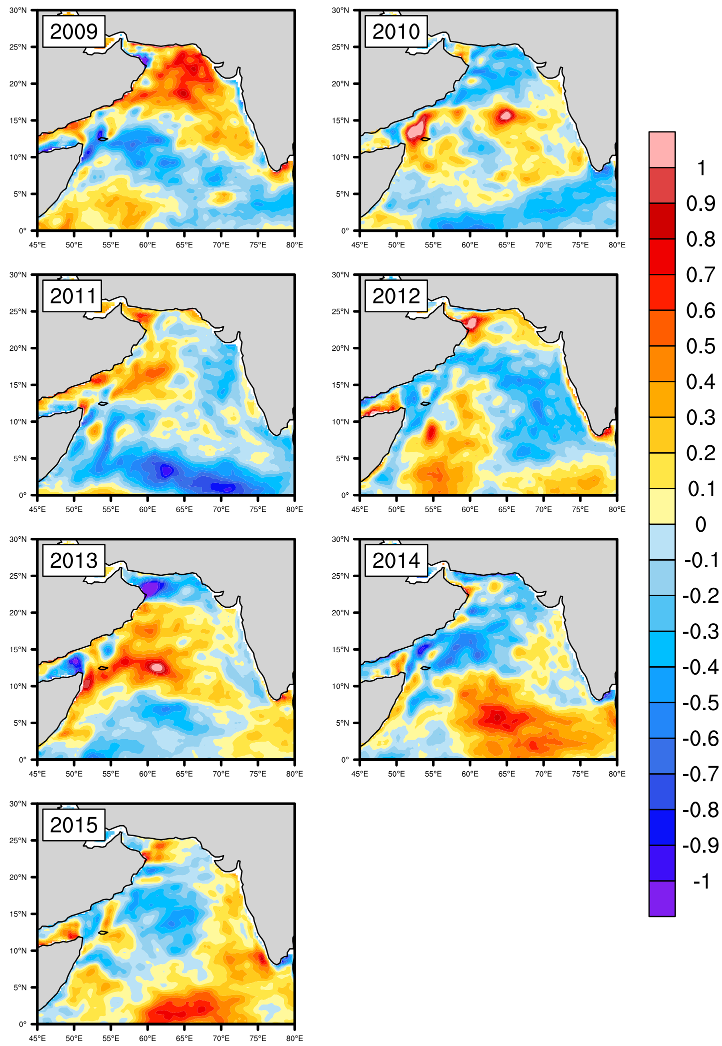


Figure A2: Yearly anomaly relative to the 7-year averaged monthly mean wind vorticity (2009-2015; May).

a disconnect between the "existing questions" and the "answers". I thus kindly ask the authors to think about this issue more, in order to make the manuscript better.

Response: [Page 2, Line 3-4, Change-Track-Mode revised manuscript] According to the suggestions, we changed "Regarding the pathways of these water masses, the mechanics are not clear."

to

"Regarding the pathways of these water masses, the movements are not well observed, and the corresponding mechanics are not clear."

Reviewer 2

I thank the authors for revising the original draft of this paper, and for responding to my first review. This second draft is an improvement on the first – in particular the comparison of the observations and the re-analysis products – although there are a few points that I think require some further work.

Response: We sincerely thank the reviewer for bringing up many vital points to help us improving the manuscript.

I agree with the authors' point, made in their response, that the hydrographic observations are useful to our understanding of water masses of the Indian Ocean. But the value of these observations, as currently presented, is still not as clear as it could be. I think that this is because the literature the authors have cited is not the most helpful or relevant. I have taken a quick look at the Lutyen et al (1983) paper, and it appears to be too general to be the sole reference for the spreading of RSW (page 2, line 4). Papers specifically on the water masses of the NW Indian Ocean should be cited. I would encourage the authors to read and consider the following:

Beal et al, 2000. Spreading of Red Sea overflow water in the Indian Ocean. JGR, 105, 8549–8564

Bower et al, 2000. Character and dynamics of the Red Sea and Persian Gulf outflows. JGR, 105, 6387–6414

Durgadoo et al, 2017. Indian Ocean sources of Agulhas leakage. JGR: Oceans, 122, 3481–3499

Han & McCreary, 2001. Modelling salinity distributions in the Indian Ocean. JGR, 106, 859–877

Prasad et al, 2001. Seasonal spreading of the Persian Gulf Water mass in the Arabian Sea. JGR, 106, 17059–17071

Prasad & Ikeda, 2002. A numerical study of the seasonal variability if Arabian Sea High-Salinity Water. JGR, 107, 3197

Prasanna Kumar & Prasad, 1999. Formation and spreading of Arabian Sea High-Salinity water mass. JGR, 104, 1455–1464

Shapiro & Meschanov, 1991. Distribution and spreading of Red Sea Water and salt lens formation in the northwest Indian Ocean. 38, 21–34.

These papers should help to better place the authors' valuable observations – for instance, the southward extension of ASHSW – into an informative context, both in the introduction and the discussion. As it stands, the main conclusion regarding water masses is that ASHSW is found a little further south in the present observations than in a climatology: I don't think that this is enough.

Response: [Page 2, Line 1-29, Change-Track-Mode revised manuscript] We read these good references, and tried to digest these informations. We added more reviewing text in the Introduction Section.

Old version:

To date, the main water masses in the IO and NWIO have been described by the scientific community (Sharma et al., 1978, Kumar and Prasad, 1999; Emery, 2001; Talley et al., 2011). For instance, three water masses were defined in NWIO as Arabian Sea High-Salinity Water (ASHSW), Persian Gulf Water (PGW) and Red Sea Water (RSW). Regarding the pathways of these water masses, the mechanics are not clear. RSW is formed near the northern side of the NWIO; therefore, according to the customary ocean ventilation theory, RSW sinks and moves southward along the isopycnal layer from the generation zone following the wind-driven current (Luyten et al., 1983). However, the applicability of the ocean ventilation theory is still unknown for the northern IO, because the surface wind reverses direction under the influence of winter monsoon (Liu et al., 2018). Meanwhile, the limited meridional extent of Indian Ocean omits the polar-to-subpolar front, which helps forming intermediate water in Pacific and Atlantic Oceans (You, 1998). In contrast, in situ potential vorticity analysis on RSW reveals that the flows generally follow the zonal direction (Beal et al., 2000). How the water mass moves is worthy further investigation. In contrast, in situ potential vorticity analysis on RSW reveals that the flows generally follow the zonal direction (Beal et al., 2000). How the water mass moves is worthy further investigation.

New version:

To date, the main water masses in the NWIO have been described by the scientific community (Sharma et al., 1978, Kumar and Prasad, 1999; Emery, 2001; Talley et al., 2011). For instance, three water masses were defined in NWIO as Arabian Sea High-Salinity Water (ASHSW), Persian Gulf Water (PGW) and Red Sea Water (RSW). The formations of ASHSW, PGW and RSW are all due to the high evaporation (Shapiro and Meschanov, 1991; Kumar and Prasad, 1999; Bower et al., 2000; Prasad et al., 2001; Prasad and Ikeda, 2002). Regarding the pathways of these water masses, the movements are not well observed, and the corresponding mechanics are not clear. Kumar and Prasad (1999) described the climatological seasonal distribution of ASHSW using in-situ temperature and salinity fields. In the northern Arabian Sea, ASHSW forms in the surface during winter, and moves southward due to the surface wind. Otherwise, the multi-scale variations of ASHSW were not sufficiently documented (Kumar and Prasad, 1999; Prasad and Ikeda, 2000). According to the customary ocean ventilation theory, ASHSW sinks and moves southward along the isopycnal layer from the generation zone following the wind-driven current (Luyten et al., 1983). However, the applicability of the ocean ventilation theory is still unknown for the NWIO, because the surface wind reverses direction under the influence of winter monsoon (Liu et al., 2018). RSW supplies important intermediate water salinity source in the entire Indian Ocean basin (Han and McCreary Jr., 2001). Formation and spreading of RSW exhibit seasonal variations (Bower et al., 2000; Beal et al., 2000). Based on the long-term hydrographic data, the occurrence of RSW show four possible branches of RSW around the Gulf of Aden: First flows eastward to the Arabian Basin, the second moves southward to Somali Basin, the third spreads southward along the Somali coast, and the fourth moves northeastward along the Arabian coast (Shapiro and Meschanov, 1991). Later, Beal et al., (2000) highlighted the branch along the Somali coast, meanwhile, the potential vorticity analysis revealed that the flows generally followed the zonal direction in NWIO. It is noted that the mechanics of intermediate water in Indian Ocean should be different from that in the Pacific and Atlantic Oceans. The limited meridional extent of Indian Ocean omits the polar-to-subpolar front, which helps forming intermediate water in Pacific and Atlantic Oceans (You, 1998). How the RSW moves is worthy further investigation (Durgadoo et al., 2017).

Besides, we cited references in the Section Results (Section 3.2 and 3.4), including Kumar and Prasad (1999), and Shapiro and Meschanov (1991).

The scientific message of the paper would be improved further if the particle tracking were better integrated with the discussion of water masses. The final paragraph of Section 3.4 still feels a little brief. As such, the scientific value of the particle tracking is not clear. Again, I would encourage the authors to discuss the results of their experiments in the context of work specific to the NW Indian Ocean, and the papers listed above should also be helpful here. Trajectories in the PGW and RSW layers are potentially very informative given the distance between the Carlsberg Ridge and the Persian Gulf/Red Sea. Plotting the temperature/salinity properties of particles at the time and location of initiation might also be very informative.
Response: We tried to show Lagrangian trajectories of water masses based on ocean reanalysis data. However, the motivation of present work is to display the onetime hydrographic survey. The systematic work on Lagrangian descriptions of PGW and RSW beyonds the main scope of present work, and leaves for future work. We tried to add the temperature information in Figure 6 (Figure A3), while the temperature information affect the visualisation of trajectory (i.e. Figure A3c–d). We finally did not add the temperature information.

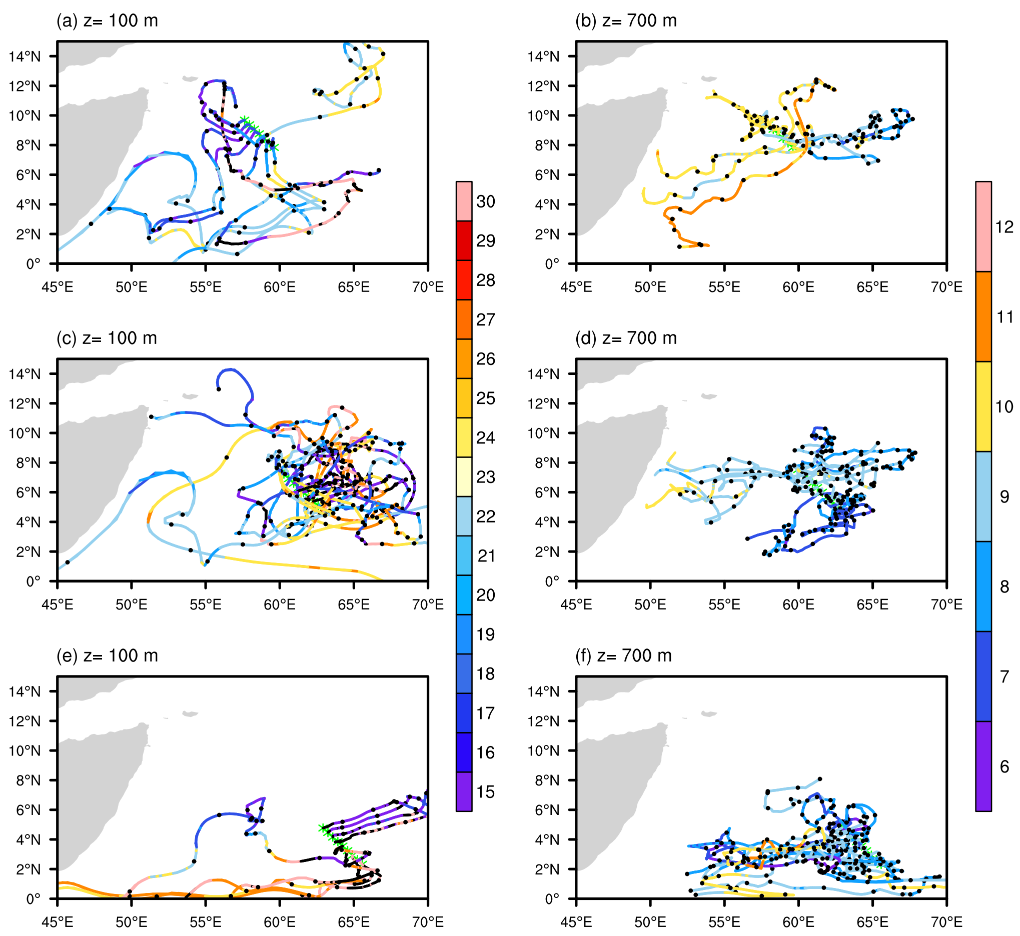


Figure A3: Trajectories of tracers, the water temperatures were added.

Regarding the interpretation of the particle trajectories, I am not convinced that the westward trajectories visible in Figure 6(e) are the result of eddy transport – surely the trajectories are too straight for this to be the case? Given the location of this westward flow and the SODA velocity distribution presented in Figure 5, is it possible that these trajectories represent transport by the WPPW?

Response: [Page 12 Line 32, Change-Track-Mode revised manuscript] We added the possible of WPPW in the hypothesis. We believe there are a lot information behind these trajectories, and the dynamics is rarely discussed here. We hope to do more research in the future.

The methods section is much clearer than in the previous draft. Now that I understand what the authors have done, I have a couple of points to raise. Firstly, I am not convinced that no calibration is required. The differences between the CTD and XCTD are, at depth, not insignificant. If the variance about the quoted mean difference in the intermediate ocean is not excessively large, I would have thought that calibration of the XCTDs against the ship's CTD would be necessary. Secondly, if Argo observations are already processed and calibrated by the Argo programme prior to being made available " and given that the distance between the Argo and CTD profiles is almost twice that between the XCTD and CTD profiles " I would have thought that this comparison could be removed: it doesn't add anything.

Response: [Page 3 Line 32-33, and Page 4 Line 1-9; Change-Track-Mode revised manuscript] We deleted the comparison between Argo and CTD. On the other aspect, for the comparison between CTD and XCTD, because the XCTD sensors are expandable, it is probably not convincing to use one XCTD error to calibrate all other XCTD. We therefore keep the other post-processing method unchanged.

Finally, I remain puzzled by the discussion about ventilation (page 8, final paragraph). Firstly, the definition of the mixed layer given in the authors' response to my first review should be included in the paper, as it is relevant to the discussion. Secondly, the authors state that north of the outcropped 22.0 kg $m^{-3}$ isopycnal, downwelling is likely occurring. But I cannot see how downwelling would produce the upward doming of the near-surface isopycnal at this location. Have the authors considered that this could be a boundary between high-salinity ASHSW in the centre of CCE1 (northern limit of the section – and it's a cold-core eddy, so we would expect upwelling in the centre?) and fresher surface water outside of the eddy (i.e. to the south)?

Response: [Page 9 Line 14-15; Change-Track-Mode revised manuscript] The definition of thermocline was adopted from Xie et al. (2002), as the 20°C isothermal line. Regarding the isopycnal layer, we simply matched the density structure as the multi-layer model, where the 22 – 22.5 kg m$^{-3}$ layer exposed to the surface, and took part in the air-sea interaction (Figure 4; density structure).

Editorial comments as previously sent to improve clarity.

Page 2.

Line 15-16. "The phase speed of west-propagating planetary waves (WPPW) is used to match the theoretical Rossby wave". This sentence is unclear. I think not "is used". Does it refer to previous work (give a reference) or to the present manuscript (move it to a better place)?

Response: [Page 3 Line 2-3; Change-Track-Mode revised manuscript] We added two references as "(Chelton and Schlax, 1996; Subrahmanyam et al., 2001)".

Lines 19-20. "interdisciplinary survey" (spellings).
Response: [Page 3 Line 6-7; Change-Track-Mode revised manuscript] Corrected.

Line 21. Not "activity". Maybe "movement" or "distribution".
Response: [Page 3 Line 8; Change-Track-Mode revised manuscript] Corrected.

Line 31. "All stations were mainly located". Either "all" or "mainly" (which means most but not all) ? but not both! Perhaps you mean "located close to the CR section".
Response: [Page 3 Line 18; Change-Track-Mode revised manuscript] Corrected.

Page 4 line 3. Better ". . stations in these comparisons . ."
Response: [Page 4 Line 7; Change-Track-Mode revised manuscript] Corrected. Later the sentence was deleted.

Page 6 Line 19. Better omit "sufficient" (what is the upwelling sufficient for?).
Response: [Page 7 Line 14; Change-Track-Mode revised manuscript] Corrected.

Line 28. "which refers to the" → "with respect to its"
Response: [Page 7 Line 23; Change-Track-Mode revised manuscript] Corrected.

Page 7 Near bottom "current is -0.38 m/s. . ." Why "-"? (presumably because westward). A magnitude must be positive.Your response to reviewer 2 refers to Maximenko et al. (2005). You should cite it here.
Response: [Page 7 Line 25-27; Change-Track-Mode revised manuscript] The sign of current magnitude was corrected. The reference was changed to "Subrahmanyam et al. (2001)". The added the citation of Subrahmanyam et al. (2001) here.

Page 8 Line 16. "and show a clear" → "suggesting a". Not "clear" because only one isotherm.
Response: [Page 9 Line 18; Change-Track-Mode revised manuscript] Corrected.

Line 27. Better "When we move forward to" → "In"
Response: [Page 9 Line 29; Change-Track-Mode revised manuscript] Corrected.

Page 10 lines 19-20. Please explain "observation-based absolute geostrophic current". Maybe you need a subsection 2.n about this. I see you have a sentence in the conclusions ? too late!
Response: [Page 11 Line 11; Change-Track-Mode revised manuscript] At the beginning of this section, "The geostrophic current" was changed to "The observation-based absolute geostrophic current".

Page 11 line 28. "The CTD and XCTD data are precise in reconstructing the three-dimensional oceanic data". This is a bold statement! The second horizontal dimension (x) is hardly measured except at the surface. So there have to be assumptions about the profiles away from the CR section.

Response: [Page 13 Line 19; Change-Track-Mode revised manuscript] Corrected. "precise" was changed to "useful".

Page 12 lines 25-29. The meaning of this sentence is unclear because the grammar is wrong. Please break it up, decide what is the most important part, give every clause a verb.

Response: [Page 14 Line 16-22; Change-Track-Mode revised manuscript] Corrected.

"Because present paper concentrates on the CR as well as the cross-ridge current, the upper 1050 m dynamics towards the upper ocean cross-ridge water transport, which is related to the deeper ocean dynamics through pressure adjustment, meanwhile, the activity of meso-scale eddy induces deeper ocean vorticity response (Rhines and Young, 1982), the results provide potential use in the future study of hydrothermal plume event."

was changed to

"Meanwhile, the upper 1050 m dynamics over CR is related to the cross-ridge water transport in upper ocean, which influences the deep ocean circulation through pressure adjustment. Therefore, the results provide potential use in the future study of hydrothermal plume."

# Hydrographic survey over the Carlsberg Ridge in May 2012

Hailun He[1], Yuan Wang[2], Xiqiu Han[2], Yanzhou Wei[1], Pengfei Lin[3], Zhongyan Qiu[2], and Yejian Wang[2]

[1]State Key Laboratory of Satellite Ocean Environment Dynamics, Second Institute of Oceanography, Ministry of Natural Resources, Hangzhou 310012, China
[2]Key Laboratory of Submarine Geosciences, Second Institute of Oceanography, Ministry of Natural Resources, Hangzhou 310012, China
[3]State Key Laboratory of Numerical Modeling for Atmospheric Sciences and Geophysical Fluid Dynamics, Institute of Atmospheric Physics, Chinese Academy of Sciences, Beijing 100029, China

**Correspondence:** Hailun He (hehailun@sio.org.cn); Xiqiu Han (xqhan@sio.org.cn)

**Abstract.** In May 2012, we conducted a hydrographic survey over the Carlsberg Ridge in the northwest Indian Ocean. In this paper, we use these station data, in combination with some free-floating Argo profiles, to obtain the sectional temperature and salinity fields, and subsequently, the hydrographic characteristics are comprehensively analyzed. Through the basic T-S diagram, three salty water masses, Arabian Sea High-Salinity Water, Persian Gulf Water, and Red Sea Water, are identified. The sectional data show a clear ventilation structure associated with Arabian Sea High-Salinity Water. The 35.8 psu salty water sinks at 6.9°N and extends southward to 4.4°N at depths around the thermocline, where the thermocline depth is in the range of 100 to 150 m. This salty thermocline extends much further south than the climatology indicates. Furthermore, the temperature and salinity data are used to compute the absolute geostrophic current over the specific section, and the results show meso-scale eddy vertical structure different from some widely used oceanic reanalysis data. We also find a west-propagating planetary wave at 6°N, and the related features are described in terms of phase speed, horizontal and vertical structures.

## 1 Introduction

The northwest Indian Ocean (NWIO) is unique compared with the other two basin-scale oceans (Pacific and Atlantic Oceans) because the dominant characteristics are monsoon driven (Schott and McCreary Jr., 2001; Schott et al., 2009). The seasonal monsoon forces the coastal current back and forth and generates the Somalia Current, which is always marked as the strongest current in the real ocean (as strong as 3.5 m $s^{-1}$). Moreover, the monsoon is strong enough to change the pattern of basin-scale circulation. The monsoon builds up a dominant meridional current in the NWIO, changing the form of the customary zonal current (as in the Pacific and Atlantic Oceans) into a meridional current. NWIO is also famous for its role in the so-called Indian Ocean Dipole (~~IOD;~~ Saji et al., 1999; Webster et al., 1999; Han et al., 2014; Chen et al., 2015), which represents the zonal gradient of sea surface temperature ~~(SST)~~ in the Indian Ocean ~~(IO)~~. As a basin-wide signal, the ~~IOD~~Indian Ocean Dipole is closely related to the ~~IO-adjacent~~Indian-Ocean-adjacent climate (Li and Han, 2015). Some studies also emphasized the distinct meso- and submeso-scale air-sea interactions in the NWIO (Vecchi et al., 2004).

To date, the main water masses in the ~~IO and~~ NWIO have been described by the scientific community (Sharma et al., 1978; Kumar and Prasad, 1999; Emery, 2001; Talley et al., 2011). For instance, three water masses were defined in NWIO as Arabian Sea High-Salinity Water (ASHSW), Persian Gulf Water (PGW) and Red Sea Water (RSW). The formations of ASHSW, PGW and RSW are all due to the high evaporation (Shapiro and Meschanov, 1991; Kumar and Prasad, 1999; Bower et al., 2000; Prasad et al., 2001; Prasad and Ikeda, 2002). Regarding the pathways of these water masses, the movements are not well observed, and the corresponding mechanics are not clear. Kumar and Prasad (1999) described the climatological seasonal distribution of ASHSW using in-situ temperature and salinity fields. In the northern Arabian Sea, ASHSW forms in the surface during winter, and moves southward due to the surface wind. Otherwise, the multi-scale variations of ASHSW were not sufficiently documented (Kumar and Prasad, 1999; Prasad and Ikeda, 2002). According to the customary ocean ventilation theory, ASHSW sinks and moves southward along the isopycnal layer from the generation zone following the wind-driven current (Luyten et al., 1983). However, the applicability of the ocean ventilation theory is still unknown for the NWIO, because the surface wind reverses direction under the influence of winter monsoon (Liu et al., 2018). RSW supplies important intermediate water salinity source in the entire Indian Ocean basin (Han and McCreary Jr., 2001). Formation and spreading of RSW exhibit seasonal variations (Bower et al., 2000; Beal et al., 2000). Based on the long-term hydrographic data, the occurrence of RSW show four possible branches of RSW around the Gulf of Aden: First flows eastward to the Arabian Basin, the second moves southward to Somali Basin, the third spreads southward along the Somali coast, and the fourth moves northeastward along the Arabian coast (Shapiro and Meschanov, 1991). Later, Beal et al. (2000) highlighted the branch along the Somali coast, meanwhile, the potential vorticity analysis revealed that the flows generally followed the zonal direction in NWIO. It is noted that the mechanics of intermediate water in Indian Ocean should be different from that in the Pacific and Atlantic Oceans. ~~Meanwhile, t~~The limited meridional extent of Indian Ocean omits the polar-to-subpolar front, which helps forming intermediate water in Pacific and Atlantic Oceans (You, 1998). How the RSW moves is worthy further investigation (Durgadoo et al., 2017).

~~RSW is formed near the northern side of the NWIO; therefore, according to the customary ocean ventilation theory, RSW sinks and moves southward along the isopycnal layer from the generation zone following the wind-driven current (Luyten et al., 1983). However, the applicability of the ocean ventilation theory is still unknown for the northern IO, because the surface wind reverses direction under the influence of winter monsoon (Liu et al., 2018) Meanwhile, the limited meridional extent of Indian Ocean omits the polar-to-subpolar front, which helps forming intermediate water in Pacific and Atlantic Oceans (You, 1998) In contrast, in situ potential vorticity analysis on RSW reveals that the flows generally follow the zonal direction (Beal et al., 2000) How the water mass moves is worthy further investigation. In contrast, in situ potential vorticity analysis on RSW reveals that the flows generally follow the zonal direction (Beal et al., 2000). How the water mass moves is worthy further investigation.~~

On the other hand, the meso-scale eddies and planetary waves are not sufficiently observed in NWIO. The historical and present Research Moored Array for African-Asian-Australian Monsoon Analysis and Prediction ~~(RAMA)~~ observation arrays are close to the equator and omit the NWIO. In situ observations in the NWIO mainly depend on Array for Real-time Geostrophic Oceanography (Argo; Riser et al., 2016; Vitale et al., 2017). However, as we show later, the number of Argo floats is still too sparse to represent the meso-scale eddy field in the NWIO. Besides, the planetary waves at-least include Rossby and Kelvin waves (Rhines, 1975; McCreary, 1985). Satellite-retrieved sea surface height are commonly used to detect the planetary waves (Chelton and Schlax, 1996), ~~however,~~while the internal dynamics of planetary wave is not sufficiently addressed. The phase speed of west-propagating planetary waves (WPPW) is used to match the theoretical Rossby wave (Chelton and Schlax, 1996; Subrahmanyam et al., 2001), nonetheless, the vertical structure of WPPW calls for vertical profiling observation (Subrahmanyam et al., 2001).

The present circumstance stimulates our effort to find more observational resources. The Carlsberg Ridge (CR) is a typical slow-spreading ridge and lies along the northwest-southeast direction in the NWIO. Recently, we conducted an ~~interdisciplinary survery~~ interdisciplinary survey on CR (Yang et al., 2016; Wang et al., 2017), and the hydrographic analysis of CR is necessary for at least three reasons. First, hydrographic survey takes a snapshot on the water mass, and gives an evidence on the ~~activity~~ movement of water mass. Second, the observation probably captures the vertical structure of meso-scale eddy or planetary wave. Third, the results could be used to evaluate the widely-used oceanic reanalysis. The trajectory of Argo float are not manually controlled; however, ship surveys could cover specified sections and have a clearer objective. Hence, this paper aims to analyze hydrographic information by combining both CR expedition and Argo floats.

## 2 Data and methods

### 2.1 In situ data description

The data for our study were collected during the Chinese cruise DY125-24 (May 2012) by the Chinese research vessel "LISIGUANG". Hydrographic observations were conducted in the region of the CR. The vertical profiles of temperature, conductivity and pressure were obtained by a calibrated SBE-19plus CTD and some expendable CTD (XCTD). The station information is shown in Fig. 1 and Table 1. All stations were mainly located ~~along~~ close to the CR section and therefore defined the regional along-section ($y$) and cross-section ($x$) coordinates. The maximum measurement depths of XCTD and Argo are 1050 and 2000 m, and therefore we limited our analysis to depth 2000 m. According to Talley et al. (2011) and Emery (2001), upper 2000 m depth covers the upper ocean (defined as 0-500 m) and the intermediate-depth ocean (defined as 500-2000 m). In our postprocessing, 13 simultaneous Argo profiles were found within a 200 km radius of the study region (Fig. 2 and Table 1).

Regarding data quality, an intercomparison between XCTD and CTD measurement was implemented in the southern tropical Indian Ocean. The XCTD station involved was located at 73.8°E and 1.7°S at 14:23 on May 4 (Coordinated Universal Time), and the counterpart CTD station was located at 73.5°E and 1.4°S a half-hour later (14:58 on May 4; distance with the XCTD station as 47.17 km). The mean differences in the recorded in situ temperature (salinity) were 0.425°C (0.058 psu) in the upper ocean and 0.051°C (0.053 psu) in the intermediate-depth ocean. It is noted that the differences among CTD and XCTD are not negligible. However, because the distance between two stations is relatively large, and the bias of XCTD is different for instrument, we does not perform instrument calibration. We later use objective analysis method and low-pass filter to smooth the data among CTD, XCTD and Argo.

~~In our postprocessing, 13 simultaneous Argo profiles were found within a 200 km radius of the study region (Fig. 2 and Table 1). The Argo float is free-floating without regular calibration; therefore, quantifying the uncertainty of Argo is relatively~~

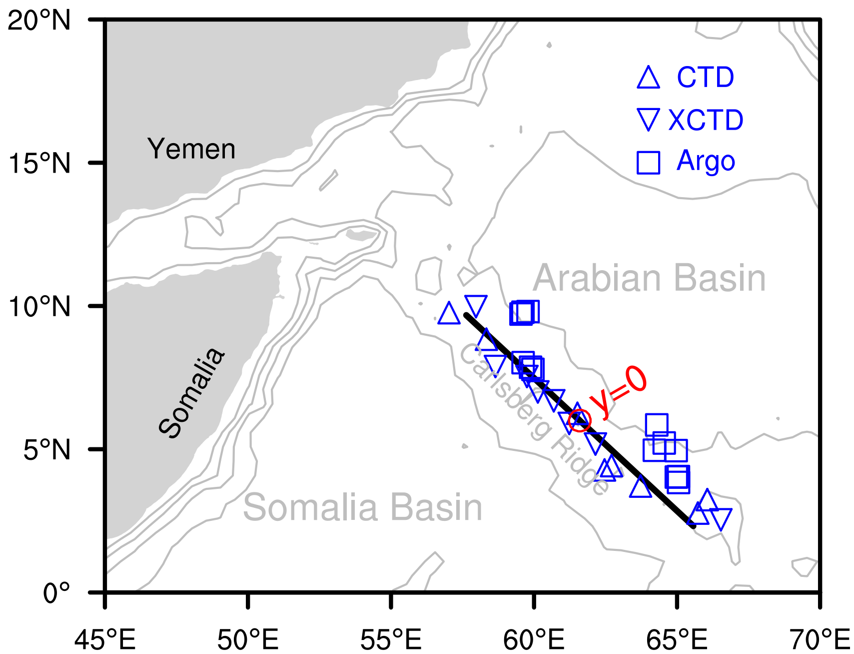


**Figure 1.** CTD/XCTD stations of the DY125-24 survey and the simultaneous Argo profiles around the CR. The CR defines local coordinates in which the $x$-coordinate is cross-track and the $y$-coordinate along-track, the corresponding origin point is selected as (61.6°E, 6.0°N), and the isobaths of -4000, -3000, -2000 and -1000 m are presented.

~~important before using the data. Fortunately, an Argo float drifted (2900877) around an XCTD station (S20CTD16; Table 1; distance with the Argo float as 79.97 km), and the two measurements occurred on May 17 and May 16, respectively. Then, we compared the XCTD with the Argo profile, and the mean differences in the in situ temperature (salinity) were 0.076°C (0.144 psu) in the upper ocean and 0.374°C (0.171 psu) in the intermediate-depth ocean. It is also noted that the differences for temperature and salinity in the intermediate depth ocean are much larger than those in the upper ocean, which is probably due to the oceanic internal high-wavenumber signals between two stations. Differences among CTD, XCTD and Argo are not negligible. However, because the distances between two stations in~~ these ~~comparisons are relatively large, and the biases of XCTD and Argo are different for instruments, we does not perform instrument calibration. We later use objective analysis method and low-pass filter to smooth the data among CTD, XCTD and Argo.~~

## 2.2 In situ data processing

All the data from several sources need to be processed to same levels because of the different sampling rates; i.e., the vertical resolutions of CTD, XCTD and Argo are 0.1, 0.1, and 2.0 m, respectively. In the first step of data postprocessing, the coarse

**Table 1.** Information on CTD/XCTD stations and Argo floats.

| Type | Station/Float | Latitude | Longitude | Time (month/day hour) |
|---|---|---|---|---|
| XCTD | S09CTD08 | 2.3°N | 66.3°E | 05/06 07 |
| XCTD | S16CTD13 | 5.1°N | 62.1°E | 05/14 16 |
| XCTD | S19CTD15 | 6.4°N | 60.4°E | 05/16 13 |
| XCTD | S20CTD16 | 7.3°N | 59.5°E | 05/16 19 |
| XCTD | S23CTD19 | 7.0°N | 60.1°E | 05/20 14 |
| XCTD | S25CTD21 | 9.6°N | 57.6°E | 05/23 04 |
| XCTD | S26CTD22 | 5.5°N | 61.1°E | 05/26 20 |
| CTD | S10CTD09 | 3.1°N | 66.0°E | 05/07 05 |
| CTD | S12CTD10 | 2.5°N | 65.4°E | 05/09 12 |
| CTD | S14CTD11 | 4.2°N | 62.3°E | 05/11 17 |
| CTD | S15CTD12 | 4.3°N | 62.4°E | 05/13 21 |
| CTD | S17CTD14 | 6.2°N | 61.3°E | 05/15 08 |
| CTD | S21CTD17 | 8.5°N | 58.2°E | 05/17 05 |
| CTD | S22CTD18 | 9.5°N | 57.0°E | 05/18 07 |
| CTD | S28CTD24 | 3.4°N | 63.4°E | 06/01 04 |
| Argo | 2901847 | 4.0°N | 65.0°E | 05/03 02 |
| Argo | 2901848 | 5.8°N | 64.3°E | 05/07 13 |
| Argo | 2900877 | 8.0°N | 59.6°E | 05/07 09 |
| Argo | 2901096 | 5.0°N | 64.2°E | 05/08 19 |
| Argo | 2901888 | 9.7°N | 59.5°E | 05/08 01 |
| Argo | 2901847 | 4.0°N | 65.0°E | 05/12 20 |
| Argo | 2901888 | 9.8°N | 59.6°E | 05/17 23 |
| Argo | 2900877 | 7.9°N | 59.9°E | 05/17 09 |
| Argo | 2901096 | 5.2°N | 64.6°E | 05/18 19 |
| Argo | 2901847 | 3.8°N | 65.1°E | 05/22 16 |
| Argo | 2900877 | 7.8°N | 60.0°E | 05/27 09 |
| Argo | 2901096 | 5.0°N | 65.0°E | 05/28 18 |
| Argo | 2901888 | 9.8°N | 59.8°E | 05/28 01 |

data are moving-averaged into a uniform vertical grid with a 5 m interval starting from 5 m below the surface. Here 5 m vertical resolution is sufficient for describing vertical structure of mixed-layer and water masses. Special treatment is imposed on one Argo float (2901888; three profiles; Table 1), where the coarse profiles lose data in the upper 20 m; thus, the missing data are filled with the same value as uppermost available data in the near surface.

The data are then projected into the standard CR section ($y$-coordinate), and the corresponding grid interval is 50 km. We use the objective analysis method to interpolate data from irregularly spaced locations to a fixed grid (Barnes, 1994). Later, a low-pass filter is imposed on the CR sectional data to remove the short-wavelength signals, which are partly from the cross-bias among different data sources and partly from the submesoscale or higher wavenumber signals in the real ocean. The low-pass filter is a two-dimensional LOcally Estimated Scatterplot Smoothing (LOESS) filter (Cleveland and Grosse, 1991), and the moving-average wavelengths are 300 km and 30 m in the horizontal and vertical directions, respectively. As a result, the smoothed data save the essential features of the thermal-salinity field but remove the noise.

### 2.3 Satellite data description

#### 2.3.1 Surface wind

We use Cross-Calibrated Multi-Platform (CCMP; Atlas et al., 2011) gridded surface vector winds here (version 2.0). CCMP data are daily products, and they are projected on $0.25^{o} \times 0.25^{o}$ grids.

#### 2.3.2 Sea surface temperature

The sea surface temperature (SST) data is produced by Operational Sea Surface Temperature and Sea Ice Analysis (OSTIA; Donlon et al., 2011), which merges satellite infrared and microwave products, ship, buoy, etc. OSTIA is daily product, and the horizontal resolutions are $0.05^{o} \times 0.05^{o}$.

#### 2.3.3 Sea surface height

For describing the sea surface height (SSH) and the related surface geostrophic current, we use the Archiving, Validation, and Interpretation of Satellite Oceanographic (AVISO) grided data. The temporal resolution is daily, and the horizontal resolutions are $0.25^{o} \times 0.25^{o}$.

### 2.4 Reanalysis data description

As references, we also employ two widely used reanalysis datasets for comparison, aiming at evaluating the quality of reanalysis data. The first reanalysis dataset is Simple Ocean Data Assimilation (SODA, version 3.3.1; Carton and Giese, 2008; Carton et al., 2018), whose horizontal resolutions are $0.25^{o} \times 0.25^{o}$ for longitude and latitude. The second reanalysis dataset is HYbrid Coordinate Ocean Model (HYCOM, version GOPS3.0:HYCOM+NCODA global 1/12$^{o}$ Reanalysis GLBu0.08/expt_19.1), and its horizontal resolutions are $0.08^{o} \times 0.08^{o}$. Both SODA and HYCOM assimilate various in situ and satellite-based data sources: historical station profiles, Argo profiles, moorings, drifters, satellite SSTs, SSHs, etc. For comparison, we extract the reanalysis datasets along the same section as the observations, and the monthly mean fields in May 2012 are used.

### 2.5 Method of tracers

Using SODA reanalysis, we release some passive tracers along the CR and backtrack their trajectories based on the Lagrangian description, and the methods are formulated by

$$\begin{cases} X^{n-1/2} & = X^{n+1/2} - U^n \cdot \Delta t \\ Y^{n-1/2} & = Y^{n+1/2} - V^n \cdot \Delta t \\ z^{n-1/2} & = z^{n+1/2} - w^n \cdot \Delta t \end{cases} \tag{1}$$

Here, $X$ and $Y$ are the Cartesian coordinates along longitude and latitude respectively, $U$ and $V$ are the corresponding currents, $z$ is the vertical coordinate, $w$ is the vertical velocity, and $n$ is the time step. In the computation, we use the three dimensional velocity ($U$, $V$, $w$) to track the tracers, and we set the time step ($\Delta t$) as 3600 s. The tracers are set along the CR on May 15, 2012, and then backward integrated to January 1, 2010.

## 3 Results

### 3.1 Background environment

The time period of the shipboard survey starts from 2012/05/06 and ends at 2012/06/01 (Table 1). Figure 2(a-c) show the monthly mean surface wind, SST and SSH, respectively. In this specific month, the summer monsoon has started but is not very strong (Fig. 2a) . The along-coast wind prevails in the regional wind field, and the wind speed in the region far from the western coast is weaker. Positive wind curl along the Somalia coast and Yemen induces ~~sufficient~~ coastal upwelling, which brings lower-layer cold water upward and cools the sea surface (Fig. 2b). The patterns of wind curl are roughly consistent with that of the climatological monthly mean wind stress curl (Beal et al., 2013). Otherwise, the wind curl in the NWIO is negative, which is consistent with the annual mean, and forces downwelling. The basin-scale semicircular SST contour (30°C) then outlines a warm area in the oceanic interior. The main part of the CR is located in this strikingly warm region (Fig. 2b).

On the other hand, SSH (or absolute dynamic height~~, ADT~~) shows multiple meso-scale eddies (Fig. 2c). There are some warm-core eddies (anti-cyclonic eddies), to the east of the CR (WCE1), east of the Horn of Africa (WCE2), and northeast of the Horn of Africa but very close to Yemen (WCE3). Two cold-core eddies (cyclonic eddies; CCE1 and CCE2) are also observed at either end of the CR. Besides, a remarkable westward current is observed at the latitude of 6°N, which is noted here as a WPPW. WPPW is pronounced compared with the circumstances around the specific region ~~, which refers to the~~with respect to its zonal extent (7.5° in longitude), while the meridional extent is relatively narrow (1.3° in latitude). The magnitude of zonal current is ~~-0.38~~ 0.38 m/s. Furthermore, we investigated the longitude-time plot of the surface zonal current at 6°N latitude ~~(surface geostrophic current from SSH; results are not shown here),~~ (Subrahmanyam et al., 2001, surface geostrophic current from SSH, results are not shown here), the WPPW is observed to start at 69°E on day 102, the surface current propagates westward with a phase speed of 0.2 m s$^{-1}$ and arrives at 60°E on day 155.

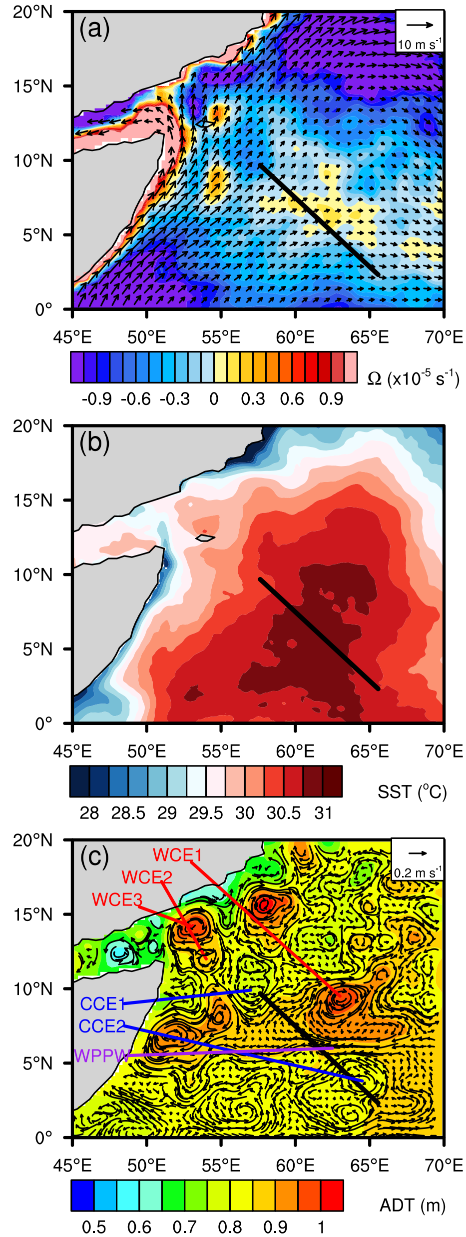


**Figure 2.** (a) Monthly mean wind vector and vorticity (Ω) from CCMP wind data, data are plotted every 3 points for wind vector; (b) monthly mean sea surface temperature from OSTIA data; and (c) monthly mean sea surface height (absolute dynamic topography), and the consistent surface geostrophic current (shown with every 2 points) from AVISO. The month of May 2012 is considered.

### 3.2 Temperature, salinity and density

First, we impose the water mass analysis on the objective-analysis data (section 2.2), and the results are shown in Fig. 3. The data support that the upper water is more saline than the Indian Equatorial Water ~~(IEW)~~ and fresher than the Arabian Sea Water ~~(ASW)~~. The observed waters are likely to be mixed ~~IEW~~Indian Equatorial Water and ~~ASW~~Arabian Sea Water. When the latitude spans from the equatorial band (2.3-5°N in the present study) to the tropical band (5-9.7°N in the present study), the salinity generally increases, consistent with the northern-side ~~ASW~~Arabian Sea Water being much more saline than the southern-side ~~IEW~~Indian Equatorial Water (Han et al., 2014), and this meridional variation in salinity is due to the different proportions of ~~IEW~~Indian Equatorial Water and ~~ASW~~Arabian Sea Water. On the northwest side, water columns contain ASHSW, which are observed as saline water at a potential density of approximately 24 kg/m$^3$ (Kumar and Prasad, 1999).

The intermediate waters from our data are projected as PGW (Prasad et al., 2001) and RSW (Beal et al., 2000; Talley et al., 2011). According to Kumar and Prasad (1999), the definition of PGW (RSW) is the density range as 26.2-26.8 kg/m$^3$ (27.0-27.4 kg/m$^3$), temperature range 13-19°C (9-11°C), and the salinity range 35.1-37.9 psu (35.1-35.7 psu).

Sectional profiles of temperature and salinity are shown in Fig. 4. The thermocline is in the depth range of 100 to 150 m (20°C isothermal line, Xie et al., 2002). From the present observation, the thermocline is nearly flat at the equatorial band and deepens northward in the tropical band. This phenomenon is also supported by the climatological data, which reveal that the sectional distribution of the thermocline is similar to a long-standing geostrophic balanced signal. In the near surface, the isothermal line of 30°C rises to the surface on the northern side ~~and show a clear~~ suggesting a ventilation structure such that subsurface water can take part in the air-sea interaction. Meanwhile, for the intermediate water, the isothermal line tilts deeper from south to north.

The striking feature of the salinity field is that a salinity tongue appears at 100 m depth, where the salty water is ASHSW (Kumar and Prasad, 1999). Climatological data show that these salty waters originate from the north side and extend southward; however, in our survey, the extent is greater. We emphasize the iso-salinity line of 35.8 psu; the southern extent can reach $y$=150 km (or 6.9°N) in climatology but -250 km (or 4.4°N) in our survey. This result means that the salty water extends southward more than 2.5° in latitude in excess of climatology. The present sectional observation also shows the salty intermediate water as PGW and RSW (Fig. 3). The observation shows slightly more saline water than climatology on the northern side, although the overall structure is mostly consistent with the climatology. In other words, the comparison implies that the year 2002 is an anomaly year for the distributions of ASHSW, PGW and RSW.

~~When we move forward to~~ In the potential density field, the appearance of the 22 kg/m$^3$ isopycnal is evident in both the snapshot and climatology. For the snapshot, the outcrop point of the 22 kg/m$^3$ isopycnal is $y$=300 km, or 7.8°N. It is worth noting that the outcrop point is near the transition point for signs of wind vorticity (Fig. 2a), and the results suggest that the ventilation is induced by surface wind. The north side of the outcrop point has negative wind vorticity, which promotes downwelling. Ventilation is highly related to the downwelling of high-salinity water and its southern extent ~~(Luyten et al., 1983)~~ (Luyten et al., 1983; Kumar and Prasad, 1999).

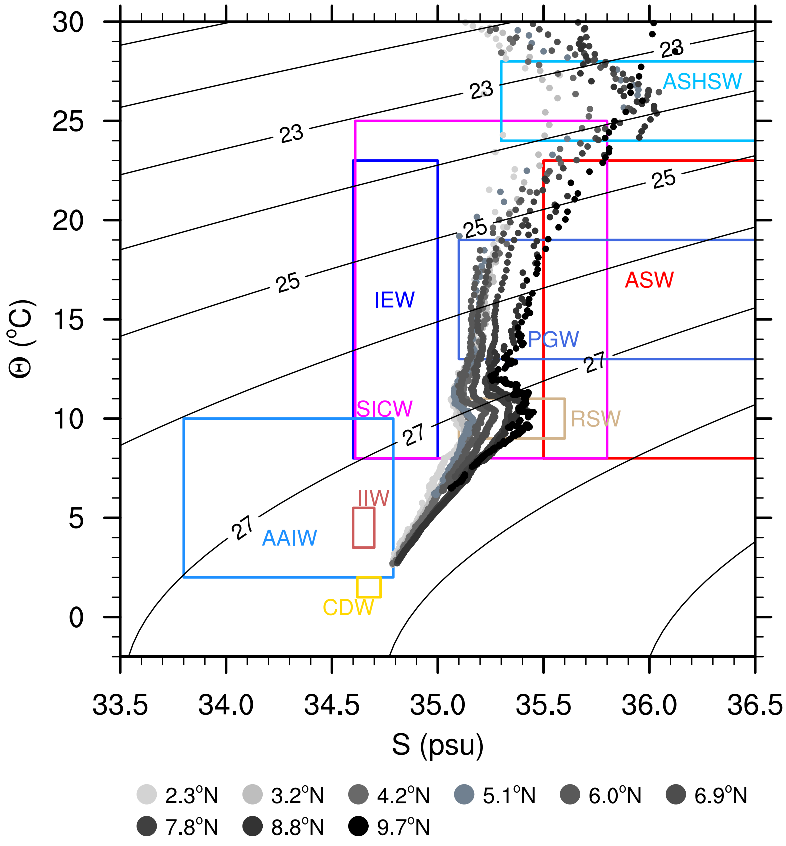


**Figure 3.** T-S diagram for the upper 2000 m of water on the CR. The water masses are defined in Emery (2001) and include the Arabian Sea water (ASW), Indian equatorial water (IEW), South Indian central water (SICW), Antarctic intermediate water (AAIW), Indonesian intermediate water (IIW), and circumpolar deep water (CDW). The rectangles represent the appropriate temperature and salinity ranges (Table 1 in Emery (2001)). Besides, Red Sea water (RSW), Persian Gulf water (PGW), and Arabian Sea High-Salinity Water (ASHSW) are also represented according to Kumar and Prasad (1999).

Fig. 4 also shows the reanalysis data, and essentially, the reanalysis captures the thermal structure quite well compared with the present observations and climatology. For instance, in the upper ocean, the surface warm water is distributed on the south side and northward to $y$=400 km where the isothermal line of 30°C crops out. The observed descending thermocline near $y$=100 km is recognizable in SODA and HYCOM. It is also noted that the equatorial near-surface upwelling in HYCOM has some evidence from the present observations. For the intermediate-depth water, in SODA and HYCOM, the isothermal lines also tilt deeper from south to north, which resembles both the present observations and the climatology.

For salinity, the southward extent of ASHSW is also captured by SODA and HYCOM, and the southward extent in HYCOM approaches the observations more closely. In the intermediate-depth water, the southward extent from the north side in SODA is similar to the observations, while the corresponding signal in HYCOM is obscured.

The upper ocean density fields from SODA and HYCOM also show clear ventilation structures. From the observations, equatorial waters with a potential density of 22 kg/m$^3$ at a depth of 30 m are rising to the surface. The outcrop points of potential density of 22 kg/m$^3$ in SODA and HYCOM are shifted southward compared with the observations. Additionally, the near-surface upwelling in the equatorial band in HYCOM is strong, but not significant in the observations.

### 3.3 Cross-track current

The observation-based absolute geostrophic current is deduced from the in situ density field by thermal wind theory (Fig. 5), where the velocity is integrated downward from the surface geostrophic current (Lagerloef et al., 1999). The velocity field is relatively strong in the upper ocean, where the current field is dominated by meso-scale eddies. The cross-track current in the equatorial band is induced by CCE2. The structure of CCE2 is asymmetric, and the positive cross-track flow is stronger than the negative counterpart. In contrast, the northwest side of CR is identified as the south part of CCE1 (northeastward flow). At 6$^{\circ}$N latitude, the vertical structure of WPPW is well rebuilt in Fig. 5a. WPPW seems to extend vertically to a depth of 200 m, and the horizontal extent is near 200 km for the current greater than 0.02 m/s. Meanwhile, the maximum cross-track current of the WPPW is 0.12 m/s. The current field also captures the northeastward current (less than 0.075 m/s) in the intermediate depth (-200 $\leq y \leq$ -20 km, and 150 $\leq y \leq$ 350 km), which is due to the corresponding isothermal tilting (Fig. 4).

For the reanalysis data, as shown in Fig. 5, although the surface currents are similar due to the assimilation of SSH in the reanalysis process, the cross-track current from reanalysis is quite different from the observation-based absolute geostrophic current. The differences are observed in three aspects. First, the meso-scale eddy CCE2 is not well represented for the vertical structure, as SODA and HYCOM limit the southern part of CCE2 to the upper 200 m, when the current speed is faster than 0.05 m/s. Meanwhile, in SODA and HYCOM, the northern part of the meso-scale eddy (CCE2) has much latitude expansion, and merges the WPPW. Second, the undercurrent in the southern portion of the observations differs from those in SODA and HYCOM. The undercurrent in SODA is relatively weak, while HYCOM shows a northward shift of the current core. Finally, for the northern portion, SODA gives a relatively shallow depth for the surface northeastward current, and the corresponding horizontal extent exceeds that of the observations. The locations of surface zero current in SODA and observation are $y$=170 and 240 km, respectively.

Part of the difference between observation-based absolute geostrophic current and reanalysis current is probably due to the near-surface Ekman current. The mean surface Ekman speed, which is approximately the difference between surface geostrophic current and in-situ surface current (from surface drifter), is within 0.1 m/s in northern ~~IO~~Indian Ocean (Saj, 2017). Besides, the climatological monthly mean mixed-layer depth in May is roughly 20 m at station 9.5$^{\circ}$N and 59.5$^{\circ}$E (on CR; Liu et al., 2018). Considering the near-surface Ekman current decays exponentially with depth, therefore, the near-surface Ekman currents in reanalysis datasets are relatively weak to affect the main results as mentioned above.

### 3.4 Tracers

Here, the SODA reanalysis supplies compact datasets for passive tracers; therefore, we set some passive tracers along the CR and backtrack their trajectories using the Lagrangian description (~~section~~Section 2.5), and the results are shown in Fig. 6. For the ASHSW, we set the tracers at a depth of 100 m, and the trajectories reveal different pathways on the CR. ~~For better describing the trajectories, we separate the CR to three latitude bands as 2.3-5°N (equatorial band), 5-8°N and 8-9.8°N. In the equatorial band (Fig. 6e), the near-equator tracers come from the west side, which is consistent with the north branch of East African Coastal Current during summer monsoon (Schott and McCreary Jr., 2001; Schott et al., 2009). Meanwhile, for the relatively north-side tracers in equatorial band, the trajectories backtrack to east side, which is probably following a westward current or meso-scale eddy~~mean flow, meso-scale eddy or WPPW. ~~While for latitudes from 5-8°N (Fig. 6c), the water mainly originates from the northeast side, and the trajectories resemble those of the ventilation theory (Luyten et al., 1983; Qiu and Huang, 1995). The results support ASHSWs are mainly from the Arabian Basin, and the southwestward flow bring the ASHSW into CR. In some occasions, the 100 m depth waters in this latitude section are from the equator, and the pathways show the north branch of East African Coastal Current and the cross-equatorial current around 66°E respectively. Similarly, the pathways start at the east of the Horn of Africa are probably due to the off-coast current at the north of Great Whirl or meso-scale eddies (Chelton et al., 2011; Wang et al., 2019). For latitudes from 8-9.8°N (Fig. 6a), the trajectories emphasis the north branch of East African Coastal Current, meanwhile, the water at the north station of CR comes from the northeast side, and one station water shows the cross-equatorial current around 53°E (east of Southern Gyre; Schott et al., 2009).~~ For better describing the trajectories, we separate the CR to three latitude bands as 8-9.8°N, 5-8°N and 2.3-5°N (equatorial band). For latitudes from 8-9.8°N (Fig. 6a), the trajectories emphasis the north branch of East African Coastal Current during summer monsoon (Schott and McCreary Jr., 2001; Schott et al., 2009), meanwhile, the water at the north station of CR comes from the northeast side, and one station water shows the cross-equatorial current around 53°E (east of Southern Gyre; Schott et al., 2009). While for latitudes from 5-8°N (Fig. 6c), the water mainly originates from the northeast side, and the trajectories resemble those of the ventilation theory (Luyten et al., 1983; Qiu and Huang, 1995). The results support ASHSWs are mainly from the Arabian Basin, and the southwestward flow bring the ASHSW into CR. In some occasions, the 100 m depth waters in this latitude section are from the equator, and the pathways show the north branch of East African Coastal Current and the cross-equatorial current around 66°E respectively. Similarly, the pathways start at the east of the Horn of Africa are probably due to the off-coast current at the north of Great Whirl or meso-scale eddies (Chelton et al., 2011; Wang et al., 2019). In the equatorial band (Fig. 6e), the near-equator tracers come from the west side, which is consistent with the north branch of East African Coastal Current. Meanwhile, for the relatively north-side tracers in equatorial band, the trajectories backtrack to east side, which is probably following a westward mean flow, meso-scale eddy or WPPW.

~~For the RSW in the intermediate-depth layer at 700 m, the trajectories in the equatorial band (Fig. 6f) show the zonal movement. Most of the trajectories move from the west side, which coincident with the potential vorticity explanation (Beal~~

~~et al., 2000), that the RSW moves southward along the coast with the help of winter monsoon, and then leave the coast and shift to middle ocean via zonal movement. Other two trajectories come from east side, and one extra trajectory moves from northwest with circular track. Hence, these trajectories display three kinds of pathways. Accordingly, in the 5-8°N band (Fig. 6d), the mainly eastward zonal movements agree with Beal et al. (2000), meanwhile, some westward trajectories resemble the ventilation theory (Luyten et al., 1983; Qiu and Huang, 1995). At last, in the 8-9.8°N (Fig. 6b), new pathway directly from northwest is emerged, and the trajectories support 700 m waters are probably directly from east of the Horn of Africa (or Gulf of Aden) without southward movements along the coast.~~

For the RSW in the intermediate-depth layer at 700 m, the trajectories show the zonal movement in the 8-9.8°N (Fig. 6b). Two trajectories move from the west side, which coincident with the potential vorticity explanation (Beal et al., 2000), that the RSW moves southward along the coast with the help of winter monsoon, and then leave the coast and shift to middle ocean via zonal movement. Meanwhile, pathway directly from northwest is emerged, and the trajectories support 700 m waters are probably directly from east of the Horn of Africa (or Gulf of Aden) without southward movements along the coast (Shapiro and Meschanov, 1991). In the 5-8°N band (Fig. 6d), the mainly eastward zonal movements agree with Beal et al. (2000), meanwhile, some westward trajectories resemble the ventilation theory (Luyten et al., 1983; Qiu and Huang, 1995). At last, in the equatorial band (Fig. 6f), most trajectories show eastward zonal movement. Other two trajectories follow westward zonal movement, and one extra trajectory moves from northwest with circular track. Hence, these trajectories display three kinds of pathways.

## 4 Discussion

The CTD and XCTD data are ~~precise~~ useful in reconstructing the three-dimensional oceanic data. Based on theoretical model, three-dimensional ocean interior can be derived using surface information (SSH and sea surface density), where the reliable mean density field is required (Lapeyre and Klein, 2006; Wang et al., 2013; Liu et al., 2014; Yan et al., 2020). In other words, for the operational purpose, the meso-scale eddy coherent structure could be built on known background density field. The Argo-only data are not sufficient to describe the meso-scale eddy in the NWIO, thus could not supply sufficient background density. In the present study, the maximum distance between Argo profiles is 500 km along the CR; however, after adding the shipboard station data, the maximum distance decreases to 100 km, which falls into the eddy-permitting scale. Sufficient sampling produces more reliable vertical structures of temperature, salinity and density.

The most remarkable signal in the upper ocean is the southward extent of ASHSW, where the counterpart in the climatology data exists but is weak in the horizontal extent. It is surprising that the HYCOM reanalysis captures the phenomenon well, while SODA shows some disadvantages. Although both SODA and HYCOM assimilate the Argo data into Oceanic General Circulation Models (OGCMs), the assimilation methods of SODA and HYCOM are considerably different. SODA adopts optimal interpolation (Carton et al., 2018), while HYCOM uses a 3D varational scheme. One advantage of a 3D variational scheme versus optimal interpolation is the conservation of dynamical constraints (Zhu et al., 2006; Yin et al., 2012; Edwards et al., 2015). Therefore, HYCOM probably describes better the wind-driven circulations, monsoon-induced coastal current and meso-scale eddy movement, which are all related to the southward extent of ASHSW. In the comparative analysis, the state-of-the-art reanalysis is still insufficient to provide good current data. Although similar sea surface dynamic heights are taken into account, the incorrect density field leads to a false vertical structure. It is also noted that the bias is probably further amplified in OGCM and leads to potential unrealistic simulations if these reanalysis data are used in the model for initialization and boundary forcing.

From the theoretical viewpoint, the phase speed of first-, second- and third-mode baroclinic Rossby wave at 6°N in Indian Ocean is roughly 0.6, 0.2 and 0.1 m/s, respectively (Subrahmanyam et al., 2001). The phase speed of WPPW match well with that of the second-mode baroclinic Rossby wave. For the generation mechanics, Subrahmanyam et al. (2001) argued that this kind Rossby wave was probably radiated from coastal trapped Kelvin wave at south-west coast of Indian. Meanwhile, this kind Rossby wave can bring wave energy from south-west coast of Indian to the Somali coast, and feed the Somali Current and Somali eddies. The present study displays the vertical structure of this kind Rossby wave, however, the dynamics of WPPW (and Rossby wave) and the its association with Somali Current and Somali eddies call for further study.

Generally, the hydrothermal plume in CR uplifts from sea bottom to water depth 2500 m (Murton et al., 2006; Wang et al., 2017). Present paper restricts the sectional study to the upper 1050 m (Fig. 4-5). Within this depth, the water is easily affected by surface forcing. However, on the basin-scale wind-driven circulation, the surface wind forcing affects deeper ocean through quasi-geostrophic instability (Rhines and Young, 1982) and meridional overturning circulation. ~~Because present paper concentrates on the CR as well as the cross-ridge current, the upper 1050 m dynamics towards the upper ocean cross-ridge water transport, which is related to the deeper ocean dynamics through pressure adjustment, meanwhile, the activity of meso-scale eddy induces deeper ocean vorticity response (Rhines and Young, 1982), the results provide potential use in the future study of hydrothermal plume event.~~ Meanwhile, the upper 1050 m dynamics over CR is related to the cross-ridge water transport in upper ocean, which influences the deep ocean circulation through pressure adjustment. Therefore, the results provide potential use in the future study of hydrothermal plume.

## 5 Conclusions

This paper reports a onetime hydrographic survey on the CR in the NWIO, where the latitudes cover the equatorial (2.3-5°N) and tropical (5-9.6°N) bands. The station CTD/XCTD sampling plus the Argo floats build the sectional structures of temperature and salinity as well as density. The striking feature is the southern extent of ASHSW from northwest of the CR in the upper ocean. Meanwhile, the temperature and density fields display clear ventilation structures. In the intermediate depth, the observations also capture the RSW at a depth near 700 m.

Furthermore, we compute the absolute geostrophic current based on the density profiles and sea surface height. The vertical structure of the cross-track current reveals strong signals of meso-scale eddies in the upper ocean and relatively weak north-eastward current in the intermediate depth. We also identify a strong westward-propagating planetary wave at a latitude of 6°N. The longitude and latitude lengths are 7.5° and 1.3° respectively. The corresponding phase speed is 0.2 m/s, and the vertically affected depth is roughly 200 m.

We further evaluate the state-of-the-art reanalysis with the present observations. As a result, because the Argo profiles and satellite SSH are assimilated into the reanalysis datasets, HYCOM and SODA show relatively good qualities for temperature, salinity and density. However, the reanalysis cross-track currents show large discrepancies compared with the absolute geostrophic current. Most importantly, HYCOM and SODA misinterpret some meso-scale eddies in the current field. Over the NWIO, the meso-scale eddies are relatively important but cannot be well described by the Argo-only data source. The present analysis shows more data source for potential data assimilation experiment. The present situation of insufficient sampling prompts more research activity in the NWIO.

To explore the pathways of ASHSW and RSW during the expedition time, we set tracers in SODA dataset at depths of 100 and 700 m, and backtrack their trajectories via three dimensional Lagrangian description. Overall, for the 100 m depth waters, the results reveal the pathways related to the north branch of East African Coastal Current and the flow from northeast side (or Arabian Basin), while for the 700 m depth waters, the trajectories mainly follow the zonal direction from either west and east sides. The results give direct-viewing descriptions and call for further dynamical investigations.

*Competing interests.* The authors declare that they have no conflict of interest.

*Acknowledgements.* This work is supported by the China Ocean Mineral Resources Research and Development Association Project (Nos. DY135-S2-1-07 and DY135-E2-1-01) and the National Natural Science Foundation of China (Nos. 41730535 and 41621064). OSTIA SST data were produced by the Meteorological Office of the United Kingdom (http://marine.copernicus.eu/). We are thankful to editor and two anonymous reviewers for their constructive suggestions and comments. WOA data were available in https://www.nodc.noaa.gov/. Daily Argo float data were downloaded from http://www.argodatamgt.org. CCMP wind were provided by Remote Sensing Systems (http://www.remss.com, version 2.0), AVISO SSH data were produced and distributed by the Copernicus Marine and Environment Monitoring Service (CMEMS) (http://www.marine.copernicus.eu), SODA were obtained from http://www.atmos.umd.edu/ ocean/, and HYCOM were downloaded from https://hycom.org/.

## References


Atlas, R., Hoffman, R. N., Ardizzone, J., Leidner, S. M., Jusem, J. C., Smith, D. K., and Gombos, D.: A cross-calibrated, multiplatform ocean surface wind velocity product for meteorological and oceanographic applications, Bull. Amer. Meteor. Soc., 92, 157–174, 2011.

Barnes, S. L.: Applications of the Barnes Objective Analysis Scheme. Part I: Effects of Undersampling, Wave Position, and Station Randomness, J. Atmos. Oceanic Technol., 11, 1433–1448, 1994.

Beal, L. M., Ffield, A., and Gordon, A. L.: Spreading of Rea Sea overflow waters in the Indian Ocean, J. Geophys. Res., 105, 8549–8564, 2000.

Beal, L. M., Hormann, V., Lumpkin, R., and Foltz, G.: The Response of the Surface Circulation of the Arabian Sea to Monsoonal Forcing, J. Phys. Oceanogr., 43, 2008–2022, 2013.

Bower, A. S., Hunt, H. D., and Price, J. F.: Character and dynamics of the Red Sea and Persian Gulf outflows, Journal of Geophysical Research: Oceans, 105, 6387–6414, https://doi.org/10.1029/1999JC900297, 2000.

Carton, J. A. and Giese, B. S.: A reanalysis of ocean climate using Simple Ocean Data Assimilation (SODA), Monthly Weather Review, 136, 2999–3017, 2008.

Carton, J. A., Chepurin, G. A., and Chen, L. G.: SODA3: A new ocean climate reanalysis, J. Clim., 31, 6967–6983, 2018.

Chelton, D. B. and Schlax, M. G.: Global observations of oceanic Rossby waves, Science, 272, 234–238, 1996.

Chelton, D. B., Schlax, M. G., and M., S. R.: Global observations of nonlinear mesoscale eddies, Progress in Oceanography, 91, 167–216, 2011.

Chen, G. X., Han, W. Q., Li, Y. L., Wang, D. X., and J., M. M.: Seasonal-to-interannual time scale dynamics of the equatorial undercurrent in the Indian Ocean, J. Phys. Oceanogr., 54, 1532–1553, 2015.

Cleveland, W. S. and Grosse, E.: Computational methods for local regression, Stat. Comput., 1, 47–62, 1991.

Donlon, C. J., Martin, M., Stark, J. D., Roberts-Jones, J., E., F., and W., W.: The Operational Sea Surface Temperature and Sea Ice analysis (OSTIA), Remote Sensing of the Environment, 116, 140–158, 2011.

Durgadoo, J. V., Rühs, S., Biastoch, A., and Böning, C. W. B.: Indian Ocean sources of Agulhas leakage, Journal of Geophysical Research: Oceans, 122, 3481–3499, https://doi.org/10.1002/2016JC012676, 2017.

Edwards, C. A., Moore, A. M., Hoteit, I., and Cornuelle, B. D.: Regional ocean data assimilation, Annual Review of Marine Science, 7, 21–42, 2015.

Emery, W. J.: Water Types and Water Masses*, in: Encyclopedia of Ocean Sciences (Second Edition), edited by Steele, J. H., pp. 291 – 299, Academic Press, Oxford, second edition edn., https://doi.org/https://doi.org/10.1016/B978-012374473-9.00108-9, 2001.

Han, W. and McCreary Jr., J. P.: Modeling salinity distributions in the Indian Ocean, Journal of Geophysical Research: Oceans, 106, 859–877, https://doi.org/10.1029/2000JC000316, 2001.

Han, W. Q., Vialard, J., McPhaden, M. J., Lee, T., Masumoto, Y., Feng, M., and DE Ruijter, W. P. M.: Indian Ocean decadal variability: A review, Bulletin of the American Meteorological Society, 95, 1679–1703, 2014.

Kumar, S. P. and Prasad, T. G.: Formation and spreading of Arabian Sea high-salinity water mass, J. Geophys. Res. Oceans, 104, 1455–1464, 1999.

Lagerloef, G. S. E., Mitchum, G. T., Lukas, R. B., and Niiler, P. P.: Tropical Pacific near-surface currents estimated from altimeter, wind, and drifter data, J. Geophys. Res.-Oceans, 104, 23 313–23 326, 1999.

Lapeyre, G. and Klein, P.: Dynamics of the Upper Oceanic Layers in Terms of Surface Quasigeostrophy Theory, Journal of Physical Oceanography, 36, 165–176, https://doi.org/10.1175/JPO2840.1, 2006.

Li, Y. L. and Han, W. Q.: Decadal sea level variations in the Indian Ocean investigated with HYCOM: Roles of climate modes, ocean internal variability, and stochastic wind forcing, J. Clim., 28, 9143–9165, 2015.

Liu, L., Peng, S., Wang, J., and Huang, R. X.: Retrieving density and velocity fields of the ocean's interior from surface data, Journal of Geophysical Research: Oceans, 119, 8512–8529, https://doi.org/10.1002/2014JC010221, 2014.

Liu, L. L., Huang, R. X., and Wang, F.: Ventilation of a monsoon-dominated ocean: Subduction and obduction in the North Indian Ocean, J. Geophys. Res. Oceans, 123, 4449–4463, 2018.

Luyten, J. L., Pedlosky, J., and Stommel, H. M.: The ventilated thermocline, J. Phys. Oceanogr., 13, 292–309, 1983.

McCreary, J. P.: Modeling equatorial ocean circulation, Annual Review of Fluid Mechanics, 17, 359–409, 1985.

Murton, B. J., Baker, W. T., Sands, C. M., and German, C. R.: Detection of an unusually large hydrothermal event plume above the slow-spreading Carlsberg Ridge: NW Indian Ocean, Geophys. Res. Lett., 33, L10608, 2006.

Prasad, T. G. and Ikeda, M.: A numerical study of the seasonal variability of Arabian Sea high-salinity water, Journal of Geophysical Research: Oceans, 107, 18–1–18–12, https://doi.org/10.1029/2001JC001139, 2002.

Prasad, T. G., Ikeda, M., and Kumar, S. P.: Seasonal spreading of the Persian Gulf Water mass in the Arabian Sea, J. Geophys. Res. Oceans, 106, 17 059–17 071, 2001.

Qiu, B. and Huang, R. X.: Ventilation of the North Atlantic and North Pacific: Subduction versus obduction, J. Phys. Oceanogr., 25, 2374–2390, 1995.

Rhines, P. B.: Waves and turbulence on a beta-plane, J. Fluid Mech., 69, 417–443, 1975.

Rhines, P. B. and Young, W. R.: Homogenization of potential vorticity in planetary gyres, J. Fluid Mech., 122, 347–367, 1982.

Riser, S. C., Freeland, H. J., Roemmich, D., Wijffels, S., Troisi, A., Belbeoch, M., Gilbert, D., Xu, J., Pouliquen, S., Thresher, A., Le Traon, P.-Y., Maze, G., Klein, B., Ravichandran, M., Grant, F., Poulain, P.-M., Suga, T., Lim, B., Sterl, A., Sutton, P., Mork, K.-A., Velez-Belchi, P. J., Ansorge, I., King, B., Turton, J., Baringer, M., and Jayne, S. R.: Fifteen years of ocean observations with the global Argo array, Nature Climate Change, 6, 145–153, 2016.

Saj, R. P.: Surface velocity estimates of the North Indian Ocean from satellite gravity and altimeter missions, International Journal of Remote Sensing, 38, 296–313, 2017.

Saji, N. H., Goswami, B. N., Vinayachandran, P. N., and Yamagata, T.: A dipole mode in the tropical Indian Ocean, Nature, 401, 360–363, 1999.

Schott, F. A. and McCreary Jr., J. P.: The monsoon circulation of the Indian Ocean, Progress in Oceanography, 51, 1–123, 2001.

Schott, F. A., Xie, S. P., and McCreary Jr., J. P.: Indian Ocean circulation and climate variability, Reviews of Geophysics, 47, RG1002, 2009.

Shapiro, G. and Meschanov, S.: Distribution and spreading of Red Sea Water and salt lens formation in the northwest Indian Ocean, Deep Sea Research Part A. Oceanographic Research Papers, 38, 21–34, https://doi.org/https://doi.org/10.1016/0198-0149(91)90052-H, 1991.

Sharma, G. S., Gouveia, A. D., and Satyendranath, S.: Incursion of the Pacific Ocean water into the Indian Ocean, Proc. Indian Acad. Sci., 87A, 29–45, 1978.

Subrahmanyam, B., Robinson, I. S., Blundell, J. R., and Challenor, P. G.: Indian ocean Rossby waves observed in TOPEX/POSEIDON altimeter data and in model simulations, International Journal of Remote Sensing, pp. 141–167, 2001.

Talley, L. D., Pickard, G. L., Emery, W. J., and S., J. H.: Descriptive physical oceanography: An introduction, Elsevier, Burlingham, 6 edn., 2011.

Vecchi, G. A., Xie, S. P., and Fischer, A. S.: Ocean-atmosphere covariability in the Western Arabian Sea, Journal of Climate, 17, 1213–1224, 2004.

Vitale, S. S., DiMarco, S. F., Seidel, H. F., and Wang, Z. K.: Circulation analysis in the northwest Indian Ocean using ARGO floats and surface drifter observations, and SODA reanalysis output, Dynamics of Atmospheres and Oceans, 78, 57–70, 2017.

Wang, J., Flierl, G. R., LaCasce, J. H., McClean, J. L., and Mahadevan, A.: Reconstructing the Ocean's Interior from Surface Data, Journal of Physical Oceanography, 43, 1611–1626, https://doi.org/10.1175/JPO-D-12-0204.1, 2013.

Wang, S., Zhu, W. J., Ma, J., Ji, J. L., Yang, J. S., and Dong, C. M.: Variability of the Great Whirl and its impacts on atmospheric processes, Remote Sensing, 11, 322, 2019.

Wang, Y. J., Han, X. Q., Petersen, S., Frische, M., Qiu, Z. Y., Li, H. M., Li, H. L., Wu, Z. C., and Cui, R. Y.: Mineralogy and trace element geochemistry of sulfide minerals from the Wocan Hydrothermal Field on the slow-spreading Carlsberg Ridge Indian Ocean, Ore Geology Reviews, 84, 1–19, 2017.

Webster, P. J., Moore, A. M., Loschnigg, J. P., and Leben, R. R.: Coupled ocean-atmosphere dynamics in the Indian Ocean during 1997-98, Nature, 401, 356–360, 1999.

Xie, S. P., Annamalai, H., Schott, F. A., and McCreary Jr., J. P.: Structure and mechanisms of south Indian Ocean climate variability, J Clim, 15, 864–878, 2002.

Yan, H., Wang, H., Zhang, R., Chen, J., Bao, S., and Wang, G.: A Dynamical-Statistical Approach to Retrieve the Ocean Interior Structure From Surface Data: SQG-mEOF-R, Journal of Geophysical Research: Oceans, 125, e2019JC015 840, https://doi.org/10.1029/2019JC015840, 2020.

Yang, G., He, H. L., Wang, Y., Han, X. Q., and Wang, Y. J.: Evaluating a satellite-based sea surface temperature by shipboard survey in the Northwest Indian Ocean, Acta Oceanologica Sinica, 35, 52–58, 2016.

Yin, X. Q., Qiao, F. L., Yang, Y. Z., Xia, C. S., and Chen, X. Y.: Argo data assimilation in ocean general circulation model of Northwest Pacific Ocean, Ocean Dynamics, 62, 1059–1071, 2012.

You, Y.: Intermediate water circulation and ventilation of the Indian Ocean derived from water-mass contributions, Journal of Marine Research, 56, 1029–1067, https://doi.org/doi:10.1357/002224098765173455, 1998.

Zhu, J., Zhou, G. Q., X., Y. C., Fu, W. W., and You, X. B.: A three-dimensional variational ocean data assimilation system: Scheme and preliminary results, Science in China Series D: Earth Sciences, 49, 1212–1222, 2006.

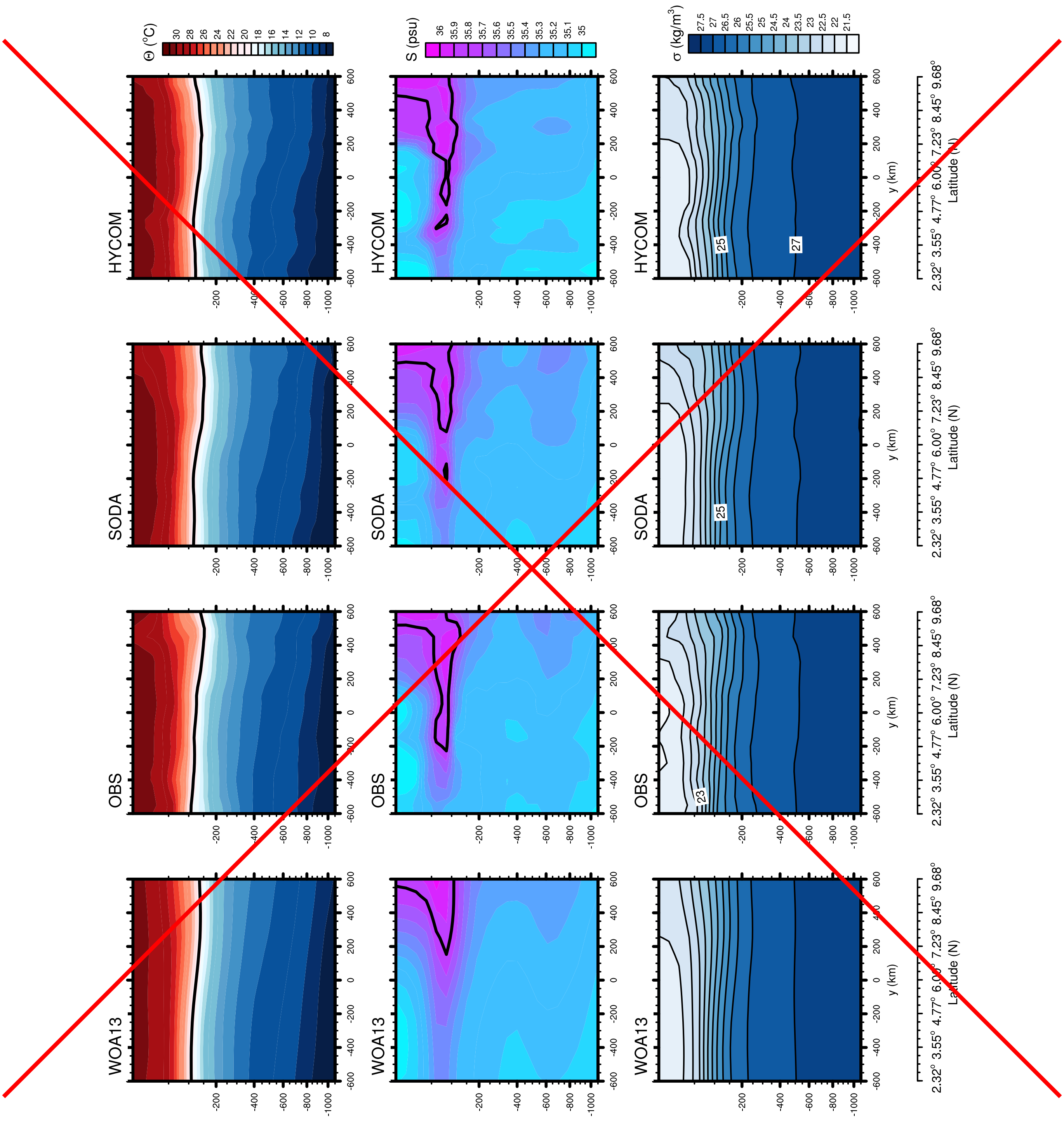


This figure is replaced.

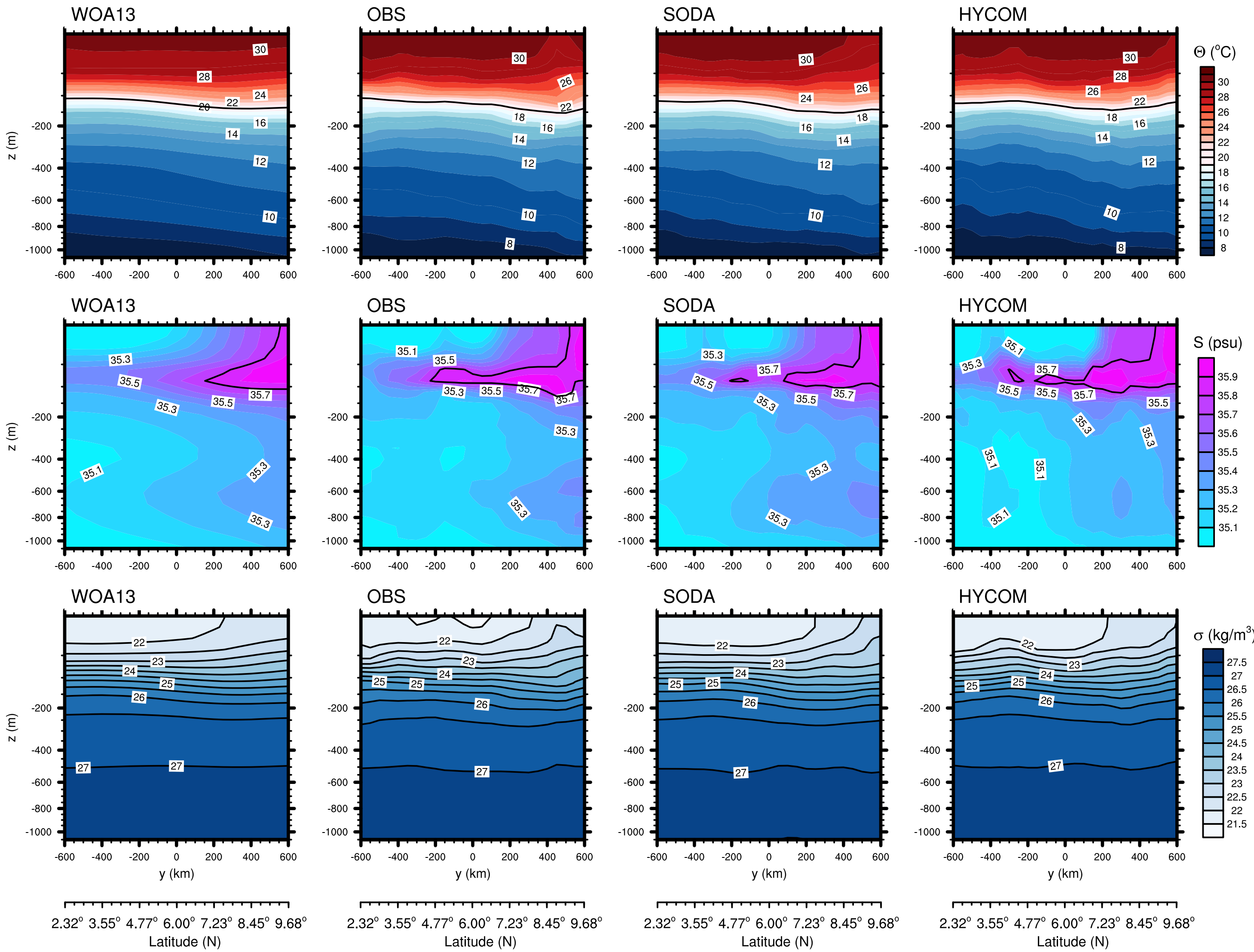


**Figure 4.** Sectional profiles of potential temperature (upper panels), salinity (middle panels) and potential density (lower panels). The data sources cover the WOA climatology (WOA13, version 2.0/A5B2, climatological monthly mean of May), the present observations, and two reanalysis datasets, SODA and HYCOM (monthly mean of May 2012). The isothermal lines of 20°C are highlighted in the potential temperatures, and the iso-salinity lines of 35.8 psu are highlighted in the salinity fields.

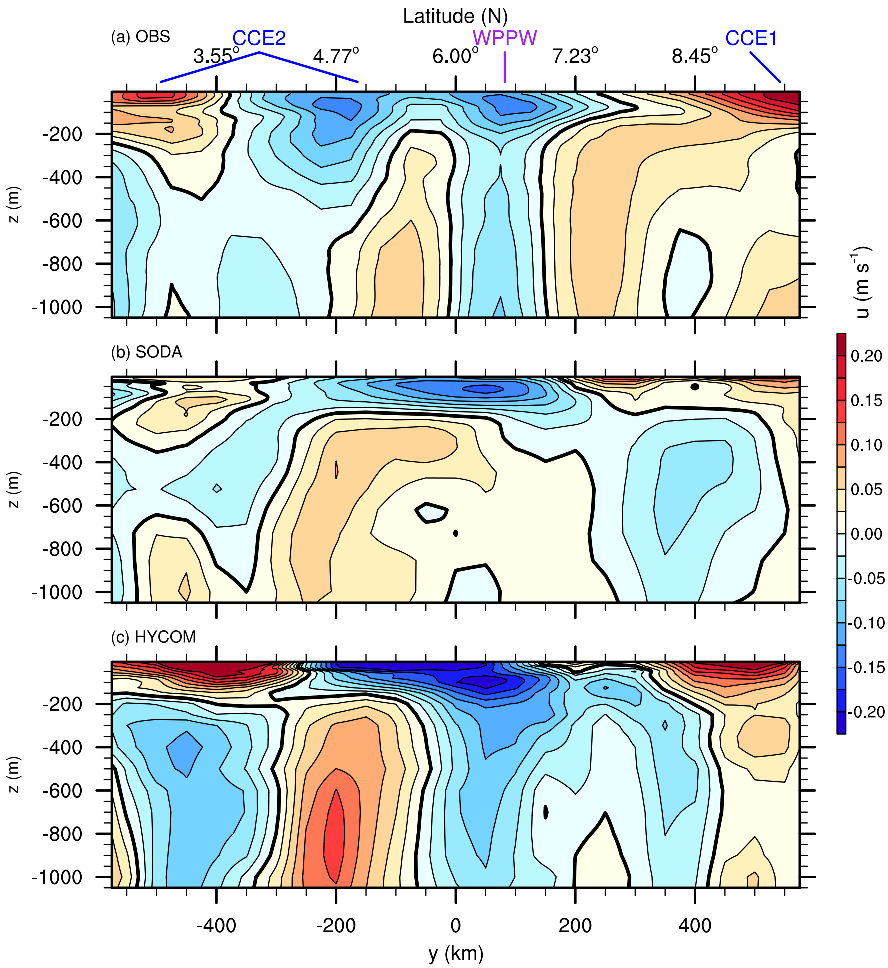


**Figure 5.** Sectional cross-track current: (a) absolute geostrophic current; (b and c) currents in SODA and HYCOM reanalysis, respectively. Northeastward current is positive. Thick black lines are the zero contours.

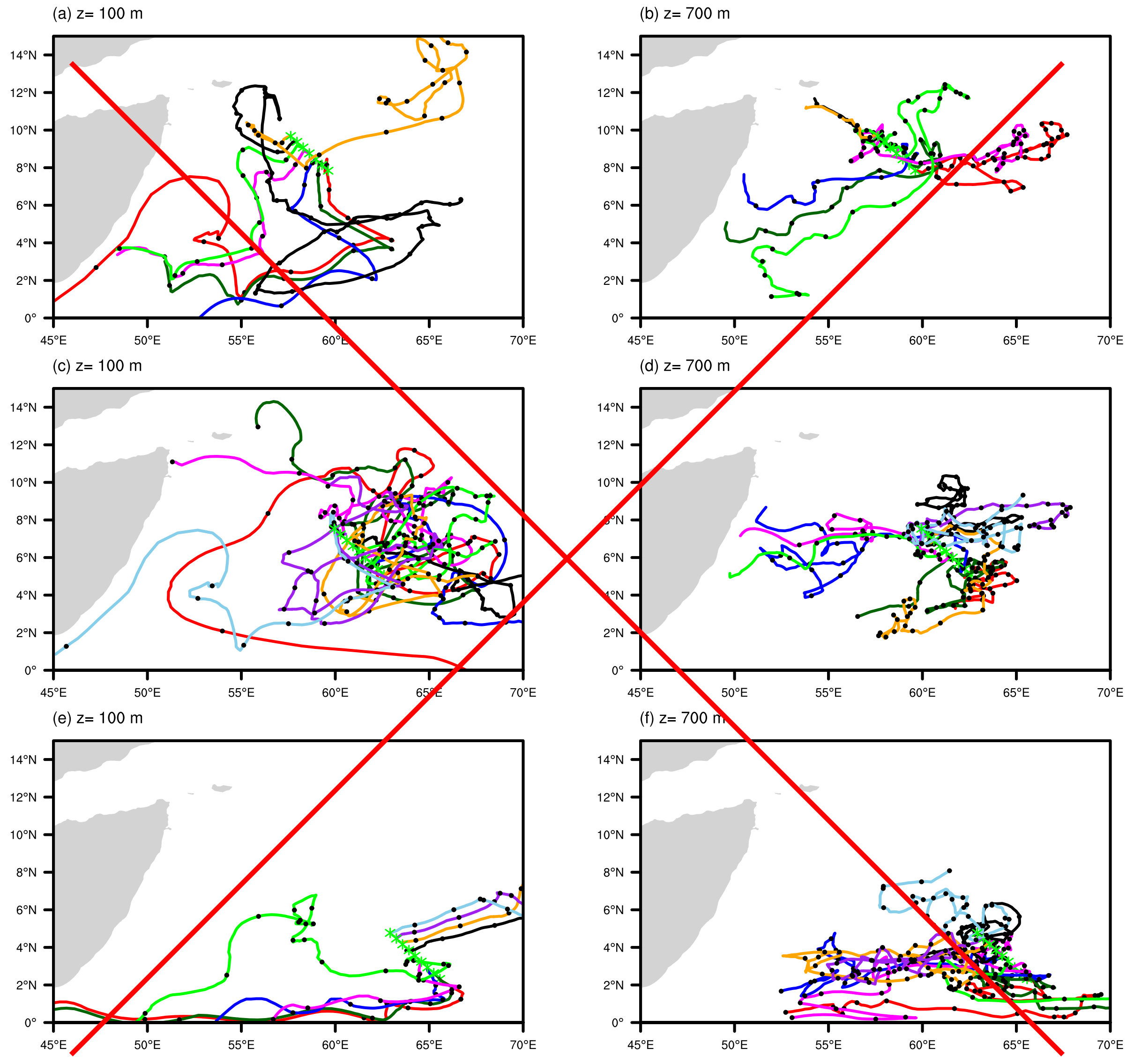


This figure is replaced.

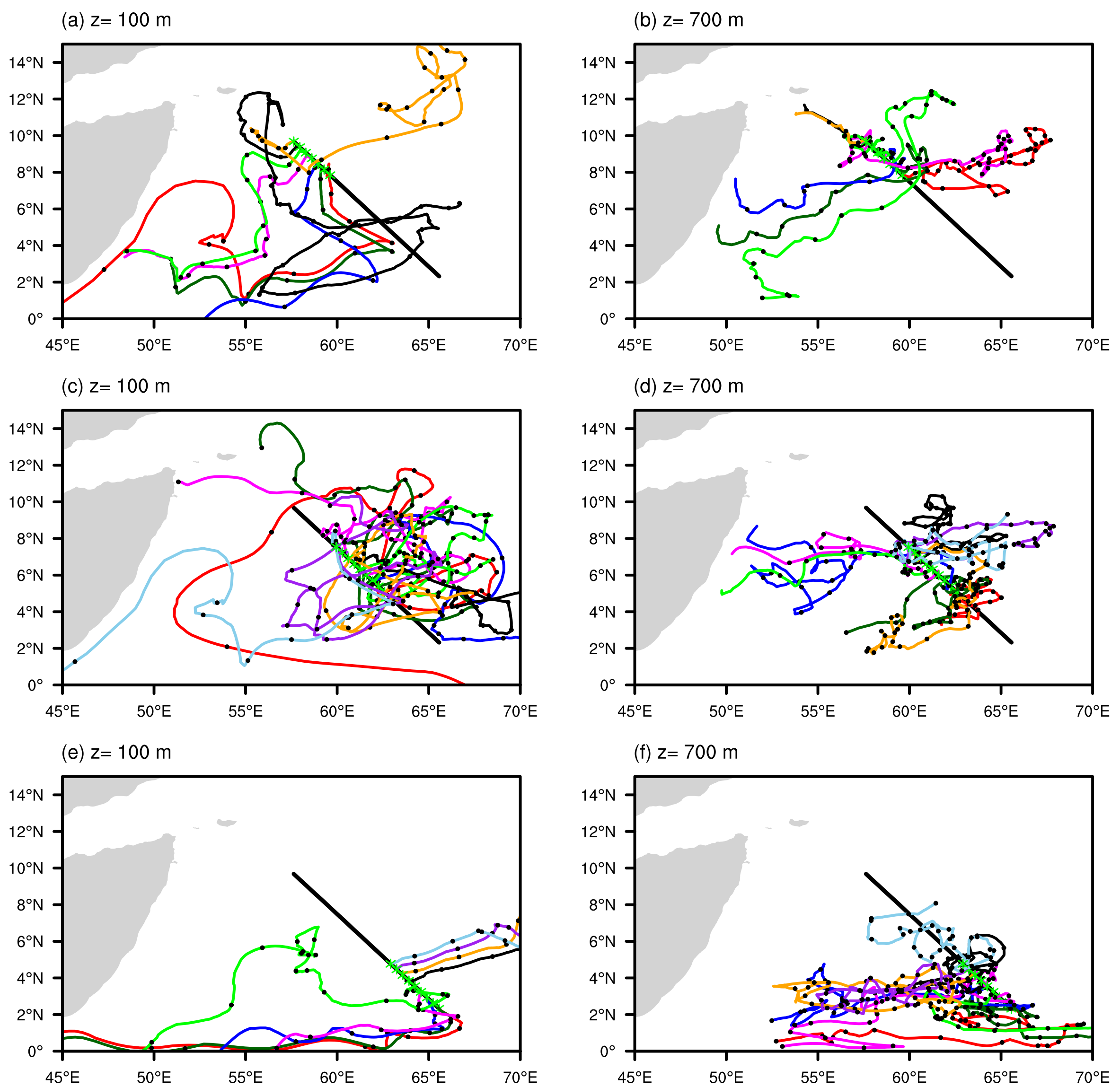


**Figure 6.** Passive tracers using SODA reanalysis. The Carlsberg Ridge is presented by black line. The tracers at May 15, 2012 are shown as green asterisks (ending points). The tracers are backtracked to January 1, 2010. The time interval is one month, as denoted by the black dots. (a-b) 8-9.8°N; (c-d) 5-8°N; (e-f) 2-5°N.